

## ARTICLE

UV Photodissociation Dynamics of  $\text{HN}_3$  in 190-248 nm<sup>†</sup>

Jian-yang Zhang<sup>a,c</sup>, Kai-jun Yuan<sup>a</sup>, Yuan Cheng<sup>a</sup>, Steven A. Harich<sup>a</sup>, Xiu-yan Wang<sup>a,c</sup>,  
Xue-ming Yang<sup>a\*</sup>, Alec M. Wodtke<sup>b</sup>

a. Dalian Institute of Chemical Physics, Chinese Academy of Sciences, Dalian 116023, China;

b. Department of Chemistry and Biochemistry, University of California at Santa Barbara, Santa Barbara 93106, USA;

c. Department of Physics, Dalian University of Technology, Dalian 116023, China

(Dated: Received on July 9, 2007; Accepted on August 2, 2007)

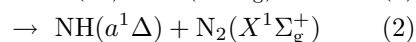
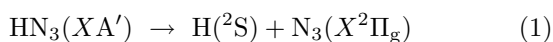
The  $\text{H}+\text{N}_3$  channel in the ultraviolet photodissociation of  $\text{HN}_3$  has been investigated from 190 nm to 248 nm using the high- $n$  Rydberg H-atom time-of-flight technique. Product translational energy distributions as well as product angular anisotropy parameters were determined for the  $\text{H}+\text{N}_3$  channel at different photolysis wavelengths.  $\text{N}_3$  vibrational state distribution has also been derived from the product translational energy distribution at these wavelengths. Above photolysis wavelength 225 nm,  $\text{HN}_3$  predominantly dissociate through the repulsive state. Below 225 nm, a new slow channel starts to appear at 220 nm in addition to the existing channel. This channel is attributed to a ring closure dissociation channel to produce the cyclic  $\text{N}_3$  product. As photolysis energy increases, this new channel becomes more important.

**Key words:** Photodissociation dynamics, H atom channel, UV photolysis, Product vibrational state distribution

## I. INTRODUCTION

The absorption spectrum of  $\text{HN}_3$  is composed of at least three absorption systems between 180-300 nm: a weak one peaking at 264.3 nm and two strong ones peaking at 204 and 190 nm, respectively [1-4]. These absorption features are broad and nearly structureless. The weak feature at  $\lambda > 220$  nm has been assigned to  $AA'' \leftarrow XA'$  [2,3,5]. At shorter wavelengths, the  $BA'$  and  $CA''$  electronic states are optically accessible, and the resulting UV absorption spectrum is strong, but no discrete structure is present.

It is known that the UV photodissociation of  $\text{HN}_3$  occurs primarily via two spin-allowed channels [1-16]:



The  $\text{NH}+\text{N}_2$  channel has been extensively studied at several different wavelengths [4,6-11].  $\text{NH}$  is produced in the lowest singlet ( $a^1\Delta$ ) instead of the  $X^3\Sigma^-$  ground state because of the spin symmetry rule. The H-atom has been investigated by Comes and coworkers by laser induced fluorescence method [12,13], and H-ion TOF spectra [14]. The average center-of-mass translation energy ( $\langle E_{\text{trans}} \rangle$ ) release has been found to be 68% of the total available energy at 248 nm. The H atom quantum yield has been measured at several wavelengths:  $\phi_{266}=0.04$ ,  $\phi_{248}=0.20$ . At 266 and 248 nm, the product anisotropy parameter is close to  $-1$ , indicating a

perpendicular electronic transition ( $AA'' \leftarrow XA'$ ). Using the H-ion TOF spectra method [14], H-N bond energy is determined to be:  $D_0(\text{H}-\text{N}_3)=30850 \pm 400 \text{ cm}^{-1}$ . The main structures observed in the distribution were assigned to a progression in the  $\nu_1$  symmetric stretching mode of  $\text{N}_3$  and the relative population of the  $(0,0,0):(1,0,0):(2,0,0):(3,0,0):(4,0,0)$  modes was found to be 0.09:0.19:0.28:0.29:0.15. Contributions to the TOF profile from other active vibrations could not be ruled out, because the resulting  $\text{H}^+$  TOF profile was poorly resolved.

Recently, the high- $n$  Rydberg H-atom time-of-flight (TOF) technique has also been employed to investigate the H-atom channel. Cook *et al.* reported the translational energy spectra of the  $\text{H}+\text{N}_3(X)$  products following excitation at eight different excitation wavelengths ( $\lambda \geq 240$  nm) [15]. Based on their experimental results and analysis, they concluded that the  $\text{N}_3$  fragments are formed in a progression of levels involving both the symmetric stretch mode ( $\nu_1, 0, 0$ ) and the symmetric stretch mode combined with one and two quanta of bending motion,  $\nu_2$ . The rotational energy disposal in the  $\text{N}_3(X)$  products was also estimated using an impulsive dissociation model, suggesting that the most probable impact parameter  $b$  is  $1.26 \pm 0.05 \text{ \AA}$ . The dissociation energy of the H-N<sub>3</sub> bond is determined to be,  $D_0(\text{H}-\text{N}_3)=30970 \pm 50 \text{ cm}^{-1}$ . The  $\text{N}_3(X)$  vibrational state population distributions are determined at eight photolysis wavelengths. Zhang *et al.* have also used Rydberg H atom TOF method to investigate the  $\text{HN}_3$  photodissociation at 248.3 and 193.3 nm [16]. At 248.3 nm, Zhang *et al.* assigned the vibrational structures in the product translational energy spectra, similar to Ref.[15]. The H-N<sub>3</sub> bond energy was determined to be  $D_0(\text{H}-\text{N}_3)=31020 \pm 180 \text{ cm}^{-1}$ . At 193.3 nm, they

<sup>†</sup>Part of the special issue "Cun-hao Zhang Festschrift".

\*Author to whom correspondence should be addressed. E-mail: xmyang@dicp.ac.cn

found that the product anisotropy parameter is clearly energy-dependent, implying multiple dissociation pathways are responsible.

The spectroscopy of  $N_3$  is rather complicated due to several interactions (Renner-Teller and spin-orbit splitting, etc.) [17-20]. Early studies demonstrated an absorption band which was attributed to an electronic transition at  $\sim 270$  nm [17]. The ground state exhibits a spin-orbit splitting of  $A_{0,\text{eff}} = -71.26$   $\text{cm}^{-1}$ , and a Renner-Teller splitting of  $\varepsilon\omega_2 = -94.38$   $\text{cm}^{-1}$  for the bending vibration. Subsequent wavelength dispersed LIF studies [18] yielded approximate values for the ground state symmetric stretch and bending vibrational frequencies of  $\omega_1 = 1320$   $\text{cm}^{-1}$  and  $\omega_2 = 457$   $\text{cm}^{-1}$  respectively. The asymmetric stretch frequency ( $\omega_3 = 1644.678$   $\text{cm}^{-1}$  [19]) has been studied by Fourier transform spectroscopy, and laser magnetic resonance [20]. Recent calculation [21] reported a linear symmetric ground state with two equal N-N bond lengths of 1.1818 Å in good agreement with the experimental value [19,20]. Meier *et al.*'s calculation showed that the  $\text{HN}_3(A)$  state PES indicates a barrier (with an estimated barrier height  $\sim 2300$   $\text{cm}^{-1}$ ) along the H-N<sub>3</sub> dissociation coordinate.

In this work, we re-investigated the photodissociation dynamics of the  $\text{HN}_3$  molecule at different wavelengths lower than 248 nm in an effort to study how the dynamics changes when the photolysis energy increases.

## II. EXPERIMENTS

The technique of H/D Rydberg atom TOF spectra technique has been described in detail elsewhere [22-24]. In this experiment, a skimmed, pulsed molecular beam of  $\text{HN}_3$ , seeded in helium (mixing ratio  $\sim 2\%$ , total pressure  $\sim 101$  kPa), is crossed perpendicularly with the photolysis laser beam. In the wavelength range of 225-280 nm, a frequency doubled dye laser (Sirah, PESC-G-24) pumped by a Nd:YAG (Spectra Physics Pro-290) is used. Laser wavelengths in the range of 188 nm to 225 nm are generated by frequency mixing of the second harmonic of the dye laser output with the Nd:YAG fundamental (1064 nm), using a second BBO crystal. The H-atom products from the photodissociation were excited to a high- $n$  Rydberg level using a two-step excitation scheme: 121.6 nm excitation to the  $n=2$  level from the ground state and the subsequent 366 nm excitation to a high- $n$  ( $n \sim 45$ ) Rydberg level from the  $n=2$  state. The 121.6 nm light was generated by four-wave mixing of two 212.5 nm photons and one 845 nm photon in a Kr/Ar mixing cell. The 212.5 nm light was generated by doubling the output of a dye laser (Sirah, PESC-G-24) operating at  $\sim 425$  nm, which was pumped by a second Nd:YAG laser (Spectra Physics Pro-290) operating at 355 nm. The 845 nm light was the direct output of a dye laser (Continue ND6000) pumped by the 532 nm output of the same Nd:YAG laser. These laser

beams were then focused into a cell with Kr/Ar mixing gas where four wave mixing at 121.6 nm was generated. The 366 nm light was generated by frequency doubling a Radiant dye laser output (Jaguar, D90MA), operating at  $\sim 732$  nm, which was pumped by a port of the 532 nm light of the same Nd:YAG laser to excite the H atoms from the  $n=2$  level to a high- $n$  Rydberg state below the ionization threshold. The two 121.6 and 366 nm laser beams were overlapped exactly in the interaction region both in space and in time. Ions and electrons formed in this region were extracted by a small electric field placed across the interaction region.

The tagged H atoms then fly away from the interaction region to reach the MCP detector. The Rydberg H atoms are efficiently ionized as soon as they pass a fine grounded metal grid in front of the MCP detector by the strong electric field applied to the front MCP plate. The total distance from the interaction region to the front face of the detector is  $\sim 333$  mm. The signal obtained is amplified by a preamplifier, discriminated by a discriminator, sent to both a digital oscilloscope for visual display and a multi-channel scaler (P7888-2(E) FASTCOMTEC) for accumulation (typically more than  $10^5$  laser shots per TOF profile) and subsequent data analysis.

$\text{HN}_3$  was prepared by heating sodium azide ( $\text{NaN}_3$ ) in excess stearic acid under vacuum for 3-4 h at 80-100 °C [24,25]. The  $\text{HN}_3$  sample was stored in a stainless steel container and He gas was filled to produce 2%  $\text{HN}_3/\text{He}$  ratio (the total pressure made up to 101-404 kPa with pure helium). Purity was checked by mass spectrometry (SRS, RGA200).

## III. RESULTS AND DISCUSSION

### A. Dissociation dynamics from 230 nm to 264 nm

The time-of-flight spectra (TOF) of the H-atom product from the photodissociation of  $\text{HN}_3$  at many different wavelengths from 230 nm to 264.3 nm were measured using the method described above. These measurements were carried out with the rotating detector direction perpendicular and parallel to the photolysis laser polarization. TOF spectra at four specific wavelengths are shown in Fig.1. Since the photolysis laser was generated using a frequency doubling scheme, the photolysis laser polarization was fixed to parallel to the molecular beam direction for convenience in this wavelength region. The TOF spectra shown in Fig.1 were then converted to the total product translational energy ( $E_{\text{trans}}$ ) distributions.

Since the total product translational energy ( $E_{\text{trans}}$ ) deposited into the two products (H and  $N_3$ ) can be written as [16,26]

$$E_{\text{trans}} = h\nu + E_{\text{int}}(\text{HN}_3) - D_0(\text{H} - \text{N}_3) - E_{\text{int}}(\text{N}_3) \quad (3)$$

where  $h\nu$  is the photon energy of the photolysis laser,

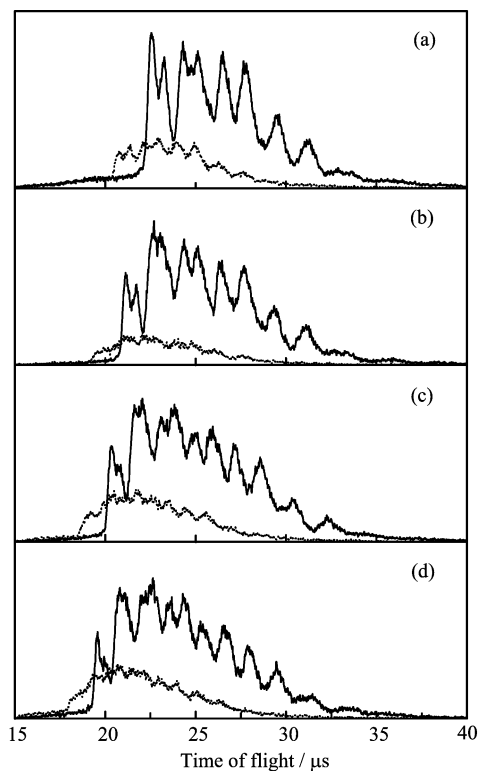


FIG. 1 TOF spectrum recorded at the photolysis wavelengths of (a)  $\lambda=248$  nm, (b)  $\lambda=240$  nm, (c)  $\lambda=235$  nm, (d)  $\lambda=230$  nm, with the MCP detector perpendicular to the laser polarization (solid lines) and parallel to the laser polarization (dotted lines).

$E_{\text{int}}(\text{HN}_3)$  is the internal energy of the HN<sub>3</sub> molecule,  $D_0(\text{H}-\text{N}_3)$  is the dissociation energy of the H-N<sub>3</sub> bond and  $E_{\text{int}}(\text{N}_3)$  is the internal energy of the N<sub>3</sub> product. HN<sub>3</sub> is cooled down to very low temperature in the supersonic expansion beam, therefore  $E_{\text{int}}(\text{HN}_3) \cong 0$ .  $E_{\text{trans}}$  can then be simplified to:

$$E_{\text{trans}} = h\nu - D_0(\text{H}-\text{N}_3) - E_{\text{int}}(\text{N}_3) \quad (4)$$

The total product translational energy distribution is also the internal energy distribution of the N<sub>3</sub> product. Thus, the structures observed in the product translational energy distribution are all due to the ro-vibrationally excited N<sub>3</sub> products. Here the photolysis energy,  $h\nu$ , is known exactly. From Eq.(4), if the maximum translational energy limit ( $E_{\text{TMAX}}$ ) in the product translational energy distribution corresponds to the N<sub>3</sub> ground ro-vibrational state,  $D_0(\text{H}-\text{N}_3)$  should be equal to  $h\nu - E_{\text{TMAX}}$ . Using the extrapolated onset of  $E_{\text{TMAX}}$  in Fig.2, the H-N<sub>3</sub> bond energy,  $D_0(\text{H}-\text{N}_3)$  is determined to be  $30910 \pm 100 \text{ cm}^{-1}$ . This result is consistent with the value obtained by Cook *et al.*,  $D_0(\text{H}-\text{N}_3) = 30970 \pm 50 \text{ cm}^{-1}$  [15] and with the value by Zhang *et al.*,  $D_0(\text{H}-\text{N}_3) = 31020 \pm 180 \text{ cm}^{-1}$  [16].

The vibrational structures observed in all the translational energy distribution at all photolysis wavelengths

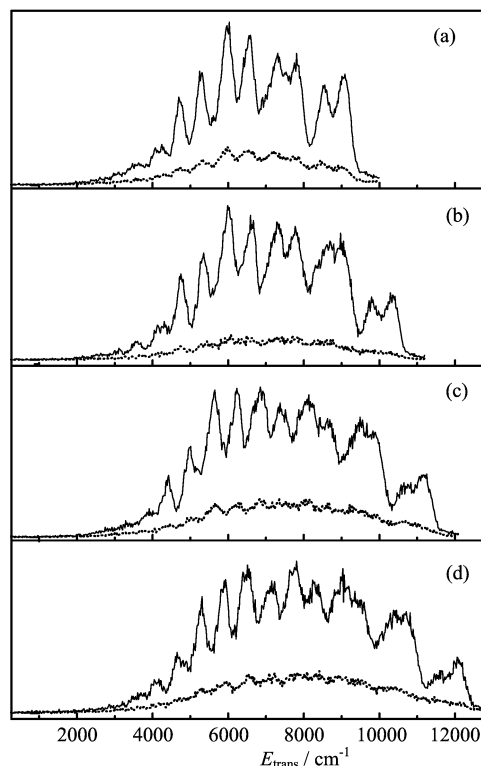


FIG. 2 The product translational energy ( $E_{\text{trans}}$ ) distribution derived from the experimentally measured H atom TOF spectra recorded at (a)  $\lambda=248$  nm, (b)  $\lambda=240$  nm, (c)  $\lambda=235$  nm, (d)  $\lambda=230$  nm, with  $\theta=90^\circ$  (dotted lines),  $0^\circ$  (solid lines).

studied here show a clear progression of doublets. These structures, given the availability of accurate theoretical vibrational term values [21], could be assigned to a progression in the N<sub>3</sub> symmetric stretching mode (characteristic spacing  $\sim 1320 \text{ cm}^{-1}$ ), ( $v_1, 0, 0$ ), together with a progression of the symmetric stretching mode with one quantum of bending motion, ( $v_1, 1, 0$ ), as did in previous similar works by Cook *et al.* [15] and Zhang *et al.* [16].

In order to understand how the nascent N<sub>3</sub> product vibrational state distribution changes with the photolysis energy, we have also carried out a wavelength dependence study of the HN<sub>3</sub> photodissociation. Figure 3 shows an experimental translational energy spectrum obtained at 235 nm. In the simulation, a full width half maximum (FWHM) of  $400 \text{ cm}^{-1}$  is used. In one of the simulation, we have included (lower panel in Fig.3) only progressions of the ( $v_1, 0, 0$ ) and ( $v_1, 1, 0$ ) vibrational series assuming only  $v_2=0, 1$  vibrational states are excited. Clearly, it is hard to simulate satisfactorily the translational energy spectrum. However, by including the series of ( $v_1, 2, 0$ ), the fitting to the translational energy spectrum is much improved (middle panel in Fig.3). This suggests that the N<sub>3</sub> products with  $v_2=2$  ( $v_1, 2, 0$ ) vibrationally excitation are also likely present. By including the three series of the vibrational states, we have successfully simulated all the translational en-

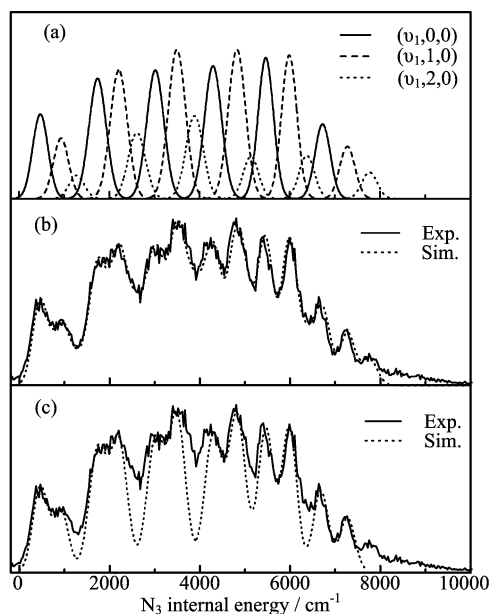


FIG. 3 Experimentally derived internal energy profiles together with simulations for photolysis of  $\text{HN}_3$  at  $\lambda=235$  nm. (a) Individual contributions of  $\text{N}_3$  vibrational state products; (b) includes progressions in the  $(v_1,0,0)$ ,  $(v_1,1,0)$  and  $(v_1,2,0)$  modes; (c) only progressions in the  $(v_1,0,0)$  and  $(v_1,1,0)$  modes are included.

ergy spectra at the photolysis wavelengths from 225 nm to 254 nm. In the translational energy spectrum shown in Fig.3, most of the  $\text{N}_3$  vibrational structures are not well resolved. However, the peak at  $\sim 7900$   $\text{cm}^{-1}$  in the translational energy distribution at the photolysis wavelength of 235 nm shown in Fig.3, which can be clearly assigned to the  $(5,2,0)$  vibrational state, strongly supports the argument that the  $(v_1,2,0)$  vibrationally excited  $\text{N}_3$  products are present.

From the translational energy distributions shown in Fig.2, the average transition energy ( $\langle E_{\text{trans}} \rangle$ ) at 230, 235, 240, and 248 nm are determined to be 64.6%, 66.5%, 68%, and 73%, respectively. The translational energy percentage decreases as photolysis energy decreases. The relative populations of  $(v_1,0,0)$  and  $(v_1,1,0)$  ( $v_1 \leq 6$ ) different vibration states were also determined and shown in Fig.4. In this figure, the relative population of the lowest vibrational state at each photolysis wavelength is normalized to one. Clearly, the vibrational excitation of the  $v_1$  mode increases as the photolysis energy increases. As photolysis energy increases, the  $v_2=1$  state population also increases relative the  $v_2=0$  state. This indicates the vibrational excitation of the  $\text{N}_3$  radical increases in both vibrational modes that are excited. It is interesting to point out, however, that the rotational excitation of the  $\text{N}_3$  product remains almost the same since the peak width in the translational energy distributions are similar in this photolysis energy regime.

Since product translational energy distributions, or

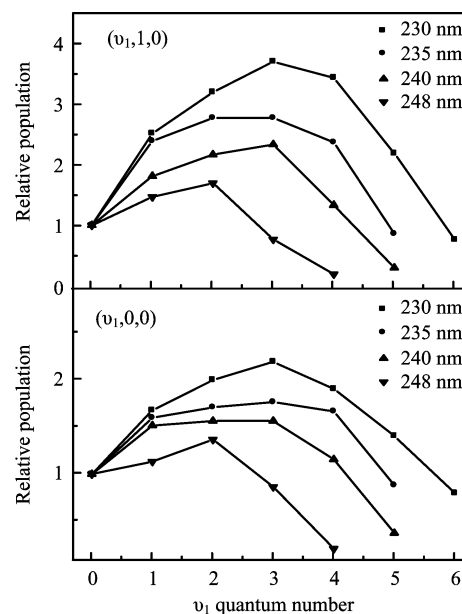


FIG. 4 Relative populations of all clearly resolved  $\text{N}_3(X)$  vibrational states at four different photolysis wavelengths were obtained for both  $(v_1,0,0)$  and  $(v_1,1,0)$  series. Here, we normalized the population of the first vibrational state to 1.

$\text{N}_3$  product internal energy distribution can be obtained, were determined at two different detection directions that are perpendicular or parallel to the photolysis laser polarizations in this experiment, product angular anisotropy parameters can also be derived.

Figure 5(a) shows the translational energy dependent product anisotropy parameter obtained for the photolysis energy of 240 nm. Between the translational energy range of 2000-11000  $\text{cm}^{-1}$ , the anisotropy parameter is between  $-0.7$  to  $-0.8$ , and is only weakly dependent on the translational energy. It is noted that anisotropy parameters below the translational energy of 2000  $\text{cm}^{-1}$  is not provided because no signal is observed in this range at the photolysis wavelengths described here. Anisotropy parameter at other photolysis wavelengths in this photolysis energy region shows similar behaviors. The overall anisotropy parameter at different photolysis wavelengths in this regime only varies slightly.

Figure 6 shows the overall angular anisotropy parameters at the photolysis wavelengths of 264.3 nm to 188 nm, in which the overall anisotropy parameters at the photolysis wavelengths from 264.3 nm to 230 nm are all around  $-0.7$ . These results suggest that the photodissociation dynamics of  $\text{HN}_3$  in this photolysis energy regime is similar, and the dissociation occurs directly via the excited potential energy surface to produce a linear  $\text{N}_3$  radical product. This conclusion is quite consistent with previous experimental results by Cook *et al.* [15] and Zhang *et al.* [16].

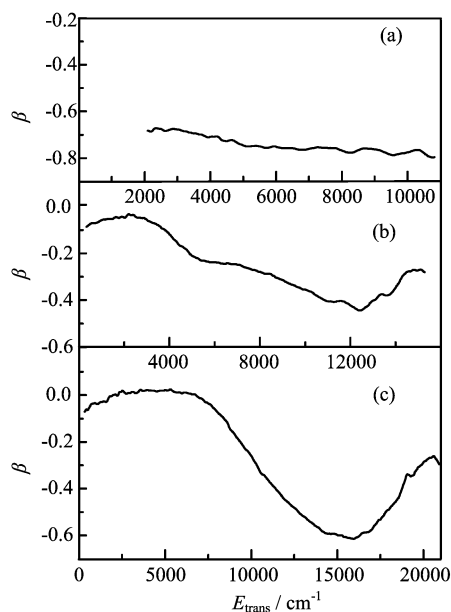


FIG. 5 Anisotropy parameter  $\beta$  as a function of the total translational energy ( $E_{\text{trans}}$ ) at three typical photolysis wavelengths: (a)  $\lambda=240$  nm, (b)  $\lambda=217$  nm, and (c)  $\lambda=193.3$  nm.

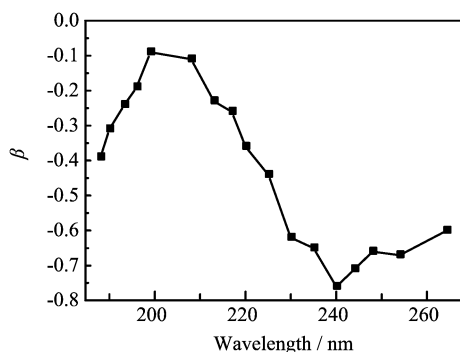


FIG. 6 The photolysis wavelength dependence of the overall angular anisotropy parameter  $\beta$ .

### B. Dynamics from 225 nm to 213 nm

Figure 7 shows that the TOF spectra of the H-atom product obtained at the photolysis wavelengths of 225, 220, 217, and 213 nm with the detector at both the perpendicular and parallel directions. Since photolysis laser wavelengths below 225 nm was generated using a frequency mixing scheme as described above, the photolysis laser polarization was fixed to be perpendicular to the molecular beam direction for convenience in this wavelength region. The TOF spectra were converted to the product translational energy distributions, and are shown in Fig.8. From this figure, the dynamical feature in the translational energy distribution starts to become a little congested and the vibrational structures eventually disappear all together at the 213 nm photodissociation. This is likely due to the larger rotational

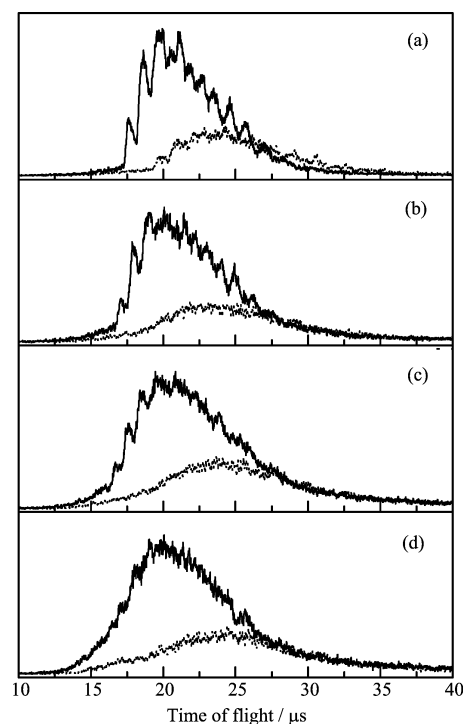


FIG. 7 TOF spectrum recorded at the photolysis wavelengths of (a)  $\lambda=225$  nm, (b)  $\lambda=220$  nm, (c)  $\lambda=217$  nm, and (d)  $\lambda=213$  nm, with the MCP detector perpendicular to the laser polarization (solid lines) and parallel to the laser polarization (dotted lines).

excitation of the  $\text{N}_3$  product because more available energy is deposited into the internal degrees of freedom of the  $\text{N}_3$  radical product. Furthermore, as the photolysis energy increases, the overall product angular anisotropy parameter decreases noticeably. From Fig.6, the overall anisotropy parameter decreases from  $-0.6$  to  $-0.1$  in this wavelength regime, suggesting the dynamics is significantly altered in this range. From the translational energy distributions shown in Fig.7, this change of the angular anisotropy can be traced to two dynamical origins: the decrease of the overall anisotropy of the main dynamical feature and the appearance of an isotropic slow component.

The most interesting change of the dynamics in this wavelength range is the appearance of a slow peak starting from 225 nm. As the photolysis energy increases, this peak seems to become more important. From the translational energy dependent anisotropy parameter at the photolysis wavelength of 213 nm (Fig.5(b)), the anisotropy parameter is almost zero in the low translational energy region. This is obviously due to the fact that the angular distribution of the slow component is isotropic. At higher translational energy, the anisotropy parameter is about  $-0.4$  at this photolysis wavelength, which is also significantly smaller than the value in the low photolysis energy region (230-248 nm). This supports our argument that the overall decrease of

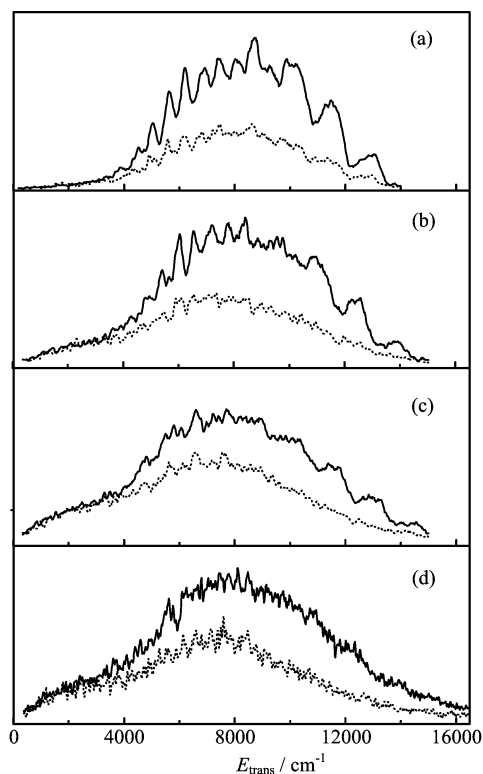


FIG. 8 The product translational energy ( $E_{\text{trans}}$ ) distribution derived from experimentally measured H atom TOF spectra at the photolysis wavelength of (a)  $\lambda=225$  nm, (b)  $\lambda=220$  nm, (c)  $\lambda=217$  nm, and (d)  $\lambda=213$  nm, with  $\theta=90^\circ$  (solid lines),  $0^\circ$  (dotted lines).

the anisotropy parameter is partly due to the anisotropy decrease of the main dynamics feature at higher translational energies.

The appearance of the slow feature in this wavelength regime turns out to be dynamically quite interesting. Recent theoretical studies show that the energy of appearance is coincident with the threshold of the ring closure pathway of the  $\text{HN}_3$  molecule, suggesting that the slow feature corresponds to the cyclic  $\text{N}_3$  product [27]. This is also consistent with the fact that the product angular distribution for this feature is isotropic.

### C. Photodissociation dynamics from 208 nm to 190 nm

TOF spectra of the H-atom product were also measured at the even shorter photolysis wavelengths. Four TOF spectra at the photolysis wavelengths of 208, 199, 193.2, and 190 nm with the detector at both the perpendicular and parallel directions to the laser polarization are shown in Fig.9. The photolysis laser polarization was also fixed to be perpendicular to the molecular beam direction for convenience in this wavelength region. The product translational energy distributions converted from these TOF are shown in Fig.10. From these translational energy distributions, translational

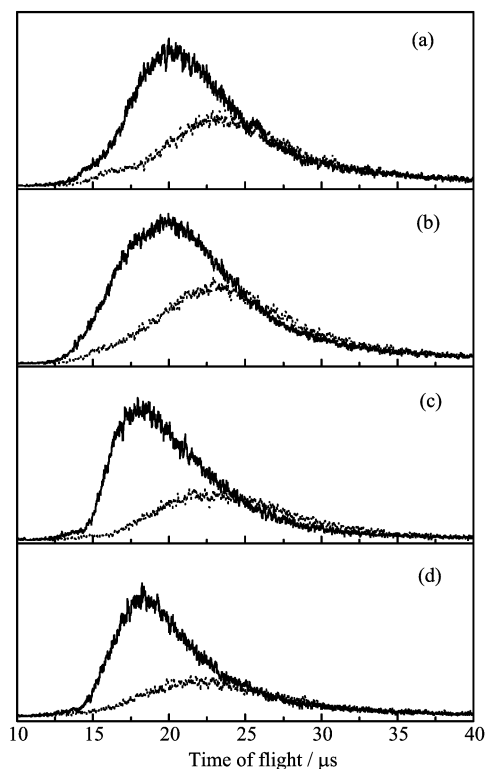


FIG. 9 TOF spectrum recorded at the photolysis wavelengths of (a)  $\lambda=208$  nm, (b)  $\lambda=199$  nm, (c)  $\lambda=193.3$  nm, and (d)  $\lambda=190$  nm, with the MCP detector perpendicular to the laser polarization (solid lines) and parallel to the laser polarization (dotted lines).

energy product anisotropy parameters can also be determined. From Fig.6, the overall product anisotropy parameter increases starting from 208 nm. Figure 5(c) shows the typical translational energy dependent anisotropy parameters at the photolysis wavelength of 193.3 nm. At the low translational energy region, the anisotropy parameter remains to be zero as in 217 nm photolysis. The increase of the overall anisotropy is due to the increase of the anisotropy of the fast component. In Fig.5(c), the maximum anisotropy parameter at higher translational energies is about  $-0.6$ , noticeably larger than that at the 217 nm photolysis. This can be likely due to that fact that different electronic states  $B$  and  $C$  are becoming accessible at shorter wavelengths.

In comparison with previous photodissociation study at 193.3 nm by Zhang *et al.* [16], noticeable difference was found in both the translational energy distribution and the energy dependent angular anisotropy between the result of this work and that by Zhang *et al.* During the experiment in this work, we found the  $\text{HN}_3$  photodissociation around 193.3 nm can easily be complicated by multiphoton processes. Therefore, we tried to lower the photolysis laser power as much as possible to reduce the multiphoton effect to minimum in the experiment.

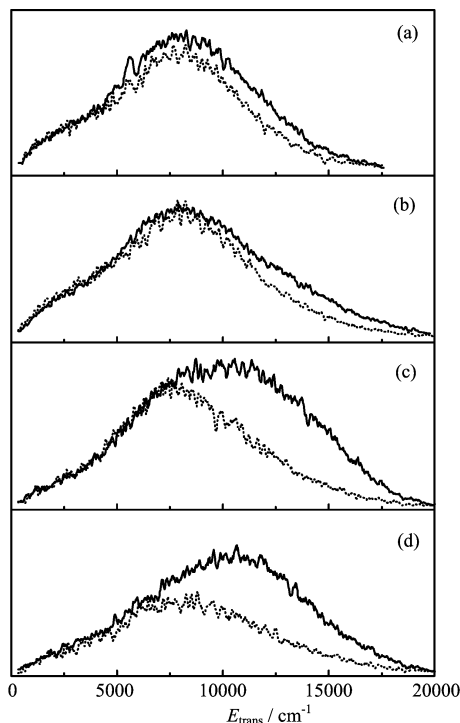


FIG. 10 The product transitional energy ( $E_{\text{trans}}$ ) distribution derived from experimentally measured H atom TOF spectra recorded at (a)  $\lambda=208$  nm, (b)  $\lambda=199$  nm, (c)  $\lambda=193.3$  nm, and (d)  $\lambda=190$  nm, with  $\theta=90^\circ$  (solid lines),  $0^\circ$  (dotted lines).

#### IV. CONCLUSION

Ultraviolet photodissociation of  $\text{HN}_3$  has been investigated in the photolysis wavelength range of 188 nm to 264.3 nm using the H-atom Rydberg tagging time-of-flight method. Time-of-flight spectra of the H atom product were measured at the detection directions both perpendicular and parallel to the photolysis laser polarization direction. Total product translational energy distributions as well as product angular anisotropy parameters were determined for the  $\text{H}+\text{N}_3$  channel at total 12 different photolysis wavelengths. The vibrational state distributions of the linear  $\text{N}_3$  product has also been derived at the photolysis wavelengths from 230 nm to 254 nm. Above photolysis wavelength 225 nm,  $\text{HN}_3$  predominantly dissociate through the repulsive state and the linear  $\text{N}_3$  product vibrational state distributions have been determined for this region. Below 225 nm, a new slow channel starts to appear in addition to the existing direct channel. The appearance energy of this channel is coincident with the theoretical energy threshold of the ring closure pathway of the  $\text{HN}_3$  molecule, suggesting that a cyclic  $\text{N}_3$  formation is likely present. At even higher photolysis energies, the change of dissociation dynamics is clearly noticeable. This is likely due to the fact that the different electronic excited states are excited at higher photolysis energies.

#### V. ACKNOWLEDGMENTS

This work was supported by Chinese Academy of Sciences via the grant of the CAS international collaboration group, and also partly by the Ministry of Science and Technology of China and the National Natural Science Foundation of China.

- [1] H. Okabe, *Photochemistry of Small Molecules*, New York: Wiley, 287 (1978).
- [2] J. R. McDonald, J. W. Rabalais, and S. P. McGlynn, *J. Chem. Phys.* **52**, 1332 (1970).
- [3] J. W. Rabalais, J. R. McDonald, V. Scherr, and S. P. McGlynn, *Chem. Rev.* **71**, 73 (1970).
- [4] A. P. Baronavski, R. G. Miller, and J. R. McDonald, *Chem. Phys.* **30**, 119 (1978).
- [5] U. Meier and V. Staemmler, *J. Phys. Chem.* **95**, 6111 (1991).
- [6] J. J. Chu, P. Marcus, and P. J. Dagdigian, *J. Chem. Phys.* **93**, 257 (1990).
- [7] F. Rohrer and F. Stuhl, *J. Chem. Phys.* **88**, 4788 (1988).
- [8] K. H. Gericke, T. Hass, M. Lock, R. Thienl, and F. J. Comes, *J. Phys. Chem.* **95**, 6104 (1991).
- [9] K. H. Gericke, M. Lock, R. Fasold, and F. J. Comes, *J. Chem. Phys.* **96**, 422 (1992).
- [10] H. H. Nelson and J. R. McDonald, *J. Chem. Phys.* **93**, 8777 (1990).
- [11] M. Hawley, A. P. Baronavski, and H. H. Nelson, *J. Chem. Phys.* **99**, 2638 (1993).
- [12] K. H. Gericke, M. Lock, and F. J. Comes, *Chem. Phys. Lett.* **186**, 427 (1991).
- [13] M. Lock, K. H. Gericke, and F. J. Comes, *Chem. Phys.* **213**, 385 (1996).
- [14] T. Haas, K. Gericke, C. Maul, and F. J. Comes, *Chem. Phys. Lett.* **202**, 108 (1993).
- [15] P. A. Cook, S. R. Langford, and M. N. R. Ashfold, *Phys. Chem. Chem. Phys.* **1**, 45 (1999).
- [16] J. Zhang, K. Xu, and G. Amaral, *Chem. Phys. Lett.* **299**, 285 (1999).
- [17] A. E. Douglas and W. J. Jones, *Can. J. Phys.* **43**, 2216 (1965).
- [18] R. A. Beaman, T. Nelson, D. S. Richards, and D. W. Setser, *J. Phys. Chem.* **91**, 6090 (1987).
- [19] C. R. Brazier, P. F. Bernath, J. B. Burkholder, and C. J. Howard, *J. Chem. Phys.* **89**, 1762 (1988).
- [20] R. Pahnke, S. H. Ashworth, and J. M. Brown, *Chem. Phys. Lett.* **147**, 179 (1988).
- [21] G. Chambaud and P. Rosmus, *J. Chem. Phys.* **96**, 77 (1991).
- [22] L. Schnieder, K. Seekamp-Rahn, E. Wrede, and K. H. Welge, *J. Chem. Phys.* **107**, 6175 (1997).
- [23] L. Schneider, W. Meier, K. H. Welge, M. N. R. Ashfold, and C. Western, *J. Chem. Phys.* **92**, 7027 (1990).
- [24] M. Qiu, Z. Ren, L. Che, D. Dai, S. Harich, X. Wang, and X. Yang, *Chin. J. Chem. Phys.* **19**, 93 (2006).
- [25] B. Krakow, R. C. Lord, and G. O. Neely, *J. Mol. Spectrosc.* **27**, 148 (1968).
- [26] J. Zhang, M. Dulligan, and C. Wittig, *J. Phys. Chem.* **99**, 7446 (1995).
- [27] J. Zhang, P. Zhang, Y. Chen, K. Yuan, S. A. Harich, X. Wang, Z. Wang, X. Yang, K. Morokuma, and A. M. Wodtke, *Phys. Chem. Chem. Phys.* **8**, 1690 (2006).